Nano Energy 41 (2017) 243–250

Contents lists available at ScienceDirect

Nano Energy

journal homepage: www.elsevier.com/locate/nanoen

Full paper

Self-assembled, highly crystalline porous ferroelectric poly(vinylidene fluoride-co-trifluoroethylene) interlayer for Si/organic hybrid solar cells

Sung Bum Kang[a], Myeong Hoon Jeong[a], In Young Choi[a], So-Dam Sohn[a], Su Han Kim[b], Hyung-Joon Shin[a], Won Il Park[b], Jae Cheol Shin[c], Myoung Hoon Song[a], Kyoung Jin Choi[a,*]

[a] School of Materials Science and Engineering, Ulsan National Institute of Science and Technology (UNIST), KIST-UNIST Ulsan Center for Convergent Materials (KUUC), Ulsan 44919, South Korea
[b] Division of Materials Science and Engineering, Hanyang University, Seoul 04763, South Korea
[c] Dept. of Physics, Yeungnam University, 280 Daehak-Ro, Gyeongsan, Gyeongbuk 38541, South Korea

ARTICLE INFO

Keywords:
Ferroelectric materials
Thin porous films
Polymers
Breath figure
Solar cells

ABSTRACT

Ferroelectric polymers can effectively improve the photovoltaic performance of solar cells, inducing an electric field to promote the dissociation of electron-hole pairs, with the thus generated charges collected from open pores. Since such performance enhancement requires materials with a unique porous crystalline structure, we herein present a novel route to highly crystalline and porous poly(vinylidene fluoride-co-trifluoroethylene) (P(VDF-TrFE)) thin films utilizing a *modified* breath figure method based on spin coating. The key feature of the above method is the addition of small amounts of water to the acetone/P(VDF-TrFE) solution to produce porous ferroelectric thin films which have significantly higher crystallinity values than nanostructures or films prepared by other methods. Furthermore, *n*-Si / poly(3,4-ethylene dioxy thiophene):poly(styrene sulfonate) hybrid solar cells with porous P(VDF-TrFE) interlayers are demonstrated to exhibit spontaneous polarization sufficient for increasing their open circuit voltages and fill factors. Finite-difference time-domain simulation reveals that the electric field due to the above spontaneous polarization increases the built-in electric field of the Schottky junction between *n*-Si and poly(3,4-ethylene dioxy thiophene):poly(styrenesulfonate) and reduces the reverse leakage current of the Schottky diode. Thus, the organic ferroelectric thin films with controlled porosity proposed in this study are well suited for a broad range of optoelectronic applications.

1. Introduction

Organic ferroelectric materials such as poly(vinylidene fluoride) (PVDF) and its copolymer with trifluoroethylene (P(VDF-TrFE)) are commonly used for fabricating non-volatile memories, ferroelectric field-effect transistors, piezoelectric energy harvesters, battery separators, microfiltration devices, etc. [1–11]. However, to achieve optimal performance in the above applications, these materials should exhibit specific morphologies and properties, e.g., be processable into pinhole-free thin films for use in ferroelectric memories and transistors to prevent electrical shorting [12]. Kang et al. employed poly(methylmethacrylate) as an additive to effectively retard the rapid crystallization of PVDF upon quenching and thus prepare thin, flat, and pinhole-free ferroelectric films with nanometer-scale crystals of β-phase PVDF [13]. Conversely, PVDF nanofibers were found to be better suited for fabricating piezoelectric energy harvesting devices than thin films, being able to accommodate larger strains and thereby afford enhanced piezoelectric power [14–16].

Recently, the enhancement of solar cell performance has been extensively attempted by incorporation of PVDF and its copolymers as interlayers. This approach requires these organic ferroelectric materials to exhibit a unique porous thin film structure, since the photogenerated electron-hole pairs must be transported through the holes of the *insulating* ferroelectric polymer. Yuan et al. [17]. achieved significant photovoltaic performance enhancement by placing a P(VDF-TrFE) interlayer between the solar cell anode and the active layer of the bulk heterojunction. The above interlayer was synthesized employing a Langmuir-Blodgett (LB) method, transferred onto the active layer, and annealed at 135 °C, which transformed the precursor continuous thin film into a nanoscale mesa structure. As a result, the interface was divided into a ferroelectric region (exerting a strong electric field) and an electrode region (enabling the flow of photogenerated charge). Therefore, control of the ferroelectric layer coverage is important for enhancing photovoltaic efficiency. In addition to proper morphology, ferroelectric polymer thin films used as solar cell interlayers should exhibit high crystallinity and ferroelectric phase content. For instance,

* Corresponding author.
E-mail address: choi@unist.ac.kr (K.J. Choi).

http://dx.doi.org/10.1016/j.nanoen.2017.09.033
Received 6 July 2017; Received in revised form 16 September 2017; Accepted 16 September 2017
Available online 20 September 2017

comparison of P(VDF-TrFE) thin films prepared using LB and spin coating methods as organic solar cell interlayers showed that despite its very small thickness of ~3 nm, the film prepared by the LB method significantly enhanced the solar cell efficiency due to its high crystallinity and ferroelectric phase content. On the other hand, the spin-coated film did not significantly improve cell efficiency due to its low crystallinity and ferroelectric content, acting as an insulator rather than as a ferroelectric material [18].

Herein, inspired by the conventional breath figure (BF) method, we describe the synthesis of highly crystalline P(VDF-TrFE) thin films with controlled porosity in the presence of a small amount of water. To the best of our knowledge, this work is the first-time report of porous P(VDF-TrFE) thin films self-assembled by spin coating and successfully used to enhance the photovoltaic performance of hybrid solar cells. The pore size and porosity of P(VDF-TrFE) thin films used as interlayers could be easily controlled by the amount of added water, influencing the photovoltaic performances of poly(3,4-ethylenedioxythiophene):poly(styrenesulfonate) (PEDOT:PSS)/Si hybrid solar cells, which were reversibly switched up and down by positive and negative poling of P(VDF-TrFE) interlayers. The mechanism responsible for the enhanced performance of PEDOT:PSS/P(VDF-TrFE)/n-Si hybrid solar cells was elucidated based on finite-difference time-domain (FDTD) simulations.

2. Experimental section

2.1. Fabrication of porous P(VDF-TrFE) thin films

Porous P(VDF-TrFE) thin films with a VDF:TrFE molar ratio of 3:1 were prepared using a solution of P(VDF-TrFE) in acetone (15 mg/mL). Addition of deionized water (18.2 MΩ cm at 25 °C) to the above solution dramatically changed the morphology of the produced films. Typically, 0.3 g of P(VDF-TrFE) was dissolved in 20 mL of acetone, followed by addition of deionized water (15–80 μL), with hydrophobic interactions between water and P(VDF-TrFE) resulting in the formation of porous P(VDF-TrFE) thin films during spin coating.

3. Characterization of P(VDF-TrFE) thin films

The morphology of P(VDF-TrFE) films was observed by scanning electron microscopy (Quanta200 FE-SEM, FEI). X-rays used in XRD measurements were generated in a Cu-closed X-ray tube at a generator voltage and current of 40 kV and 30 mA (D8 ADVANCE, Bruker AXS). FT-IR spectra (670, Varian) were acquired in attenuated total reflectance mode using a mercury cadmium telluride detector. AFM and PFM measurements were performed using an atomic force microscope (XE70, Park System). For PFM phase images, patterns were written in the contact mode with an electrical bias applied to the probe on the surface. A scan rate of 0.9 Hz, an AC frequency of 16.786 kHz, and an amplitude of 1.5 V were used. Conductive Pt-coated Si cantilevers (SCM-PIT, Bruker) were used to write and image the ferroelectric domains. The porosity of P(VDF-TrFE) films was calculated from several SEM images of porous P(VDF-TrFE) films using Image J software (NIH, http://rsb.info.nih.gov/ij).

4. Device fabrication and characterization

P(VDF-TrFE)/water/acetone solutions were spin coated onto the surface of n-Si (100) substrates (Czochralski-grown, 525 ± 25 μm thick, 1–10 Ω cm, Unisill Inc.) followed by 4-h annealing at 140 °C on a hotplate. A highly conductive PEDOT:PSS (CLEVIOS PH 1000) solution containing 9 wt% ethylene glycol and 0.1 wt% Triton X-100 was spin coated onto porous P(VDF-TrFE)/Si substrates, and the produced PEDOT:PSS/P(VDF-TrFE)/Si composites were annealed at 125 °C for 10 min. A silver electrode was deposited on top of the PEDOT:PSS layer using a shadow mask (Areal coverage ≈ 10%, 950 μm of spacing between the silver contacts) and an e-beam evaporator. Ti(20 nm)/Au (200 nm) was deposited onto Si substrates as a bottom contact. The active area of the fabricated devices equaled 0.7 × 0.7 cm^2. All devices were characterized under simulated AM 1.5 G illumination (100 mW/cm^2) using a xenon lamp solar simulator.

4.1. FDTD simulation of PEDOT:PSS/P(VDF-TrFE)/Si solar cells

The electrostatic potential energy in PEDOT:PSS/P(VDF-TrFE)/Si solar cells was calculated using COMSOL Multiphysics modeling software equipped with semiconductor, AC/DC, and piezoelectric modules. In this simulation, the Ti/Au back contact was included, but Ag top electrode was not considered because PEDOT:PSS can act as an electrode as well as a hole transfer layer in the Schottky junction. Boundary conditions for Si, Schottky contacts, and P(VDF-TrFE) ferroelectric thin films are described elsewhere [17,19], with details provided in the Supporting information.

5. Results and discussion

Porous P(VDF-TrFE) thin films with controlled porosity were self-assembled in the presence of water, as shown in Fig. 1. Sarazin et al. suggested that P(VDF-TrFE) dissolved in acetone features randomly oriented fibrous domains [20]. The synthetic approach to porous organic ferroelectric thin films proposed in this study was inspired by the BF method, wherein a polymer solution in a volatile solvent is drop cast and evaporated in a flow of humid air to enable the simultaneous absorption of water vapor by the polymer. The absorbed water vapor condenses and engages into hydrophobic interactions with the polymer, forming water droplets with sizes ranging from a few hundred nanometers to several micrometers. Eventually, a porous polymeric film with a thickness of several micrometers is formed upon complete

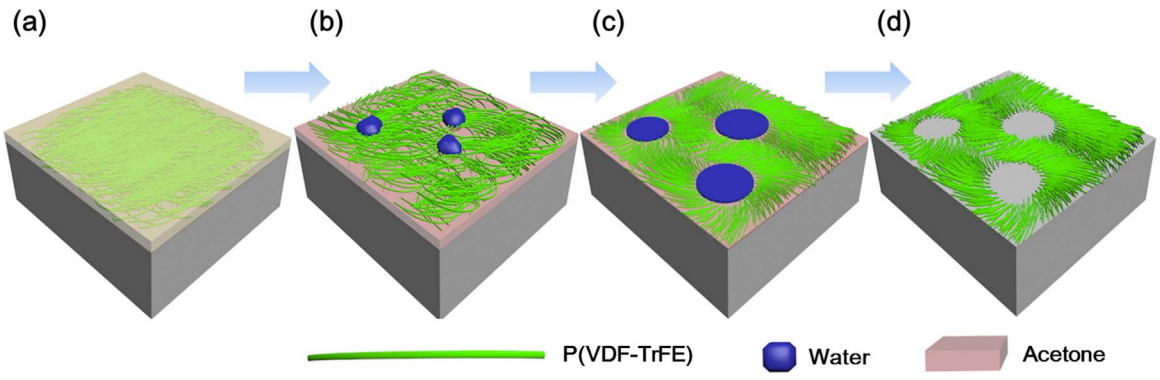

Fig. 1. Schematic fabrication of P(VDF-TrFE) porous thin films. (a) Homogenous solution of P(VDF-TrFE) and water in acetone, (b) coalescing water droplets in solution, (c) expansion of coalesced water droplets during spin coating, and (d) self-assembled porous ferroelectric P(VDF-TrFE) thin film after complete evaporation of all solvents.

solvent and moisture evaporation. The large thickness of the drop-cast polymer film implies that the produced pores are not necessarily interconnected to provide a pathway from the polymer surface to the interface with the substrate (Fig. S1**a**, Supporting information) [21,22]. On the other hand, if spin coating is used instead of drop casting, the fast solvent evaporation leaves insufficient time for water absorption from humid air. As a result, the polymer film does not adopt a perforated hole structure despite having a thickness of only ~100 nm (Fig. S1**b**) [23]. Therefore, we herein propose a *modified* spin-coating-based BF method, overcoming the limitations of the conventional technique and forming porous thin films by adding a small amount of water to the solution of P(VDF-TrFE) in acetone used for spin coating (Fig. 1**a**). The hydrophobic interaction of the added water with P(VDF-TrFE) causes the formation and growth of water droplets (Fig. 1**b and c**), producing a uniform porous P(VDF-TrFE) thin film (Fig. 1**d**). Compared to the conventional BF method, the amount of added water not only controlled the pore size of the P(VDF-TrFE) thin film and its porosity, but also allowed the formation of a completely perforated pore structure. For example, ~300-nm pores started to develop at an added water content of 0.25 wt% (Fig. S2**a and e**), with the observed porosity equaling 5%. Increasing water content increased both pore size and porosity (Fig. S2**b, c, f, and g**), i.e., ~4 μm pores and 80% porosity were observed at a water content of 0.92 wt% (Fig. S2**d and h**).

The effects of water content on the morphology and properties of P(VDF-TrFE) thin films were investigated by scanning electron microscopy (SEM), X-ray diffraction (XRD), and Fourier transform infrared (FT-IR) spectroscopy. Water-free P(VDF-TrFE) formed continuous thin films featuring random nanoneedle-shaped domains, in agreement with previous studies (Fig. 2**a**) [24–26]. In contrast, the addition of water induced the formation of a porous structure with each domain aligned in the radial pore direction (Fig. 2**b**). This behavior was explained by the hydrophobic interaction between water and P(VDF-TrFE) that resulted in the reduction of contact area and total energy by orienting P(VDF-TrFE) domains in the radial direction with respect to water droplets in the pores. Therefore, porous P(VDF-TrFE) thin films exhibited extended crystalline domains, whereas continuous films possessed shorter ones (Fig. 2**c and b**). Fig. 2**e** shows the XRD patterns of continuous and porous P(VDF-TrFE) films, with sharp peaks corresponding to β-phase (110/200) reflections at $2\theta \approx 20^{\circ}$. The narrower peaks of the porous film indicated its higher crystallinity compared to that of the continuous film. For more quantitative analysis, the XRD spectra were deconvoluted into crystalline (C) and non-crystalline (N) peaks, with the degree of crystallinity calculated as the C/(N + C) peak area ratio. The above parameter equaled 63% for the porous film, being much higher than the value of 41% observed for the continuous film. Moreover, as shown in Fig. 2**f**, porous P(VDF-TrFE) thin films exhibited crystallinities much higher than those of PVDF and its copolymer films prepared by methods such as stretching [27], poling [28], gamma-ray irradiation [29], and electrospinning [30,31] with the higher β-phase content of porous P(VDF-TrFE) thin films also confirmed by FT-IR spectroscopy (Fig. S3). Considering that the only factor accounting for the difference between continuous and porous P(VDF-TrFE) thin films is the addition of water, the much higher crystallinity and β-phase content of porous thin films can be explained by the fact that their fibrous domains are radially aligned with respect to the pores and closely packed, causing the alignment and reinforcement of the β-phase polarization direction, respectively.

Fig. 3 shows atomic force microscopy (AFM)-determined topographies and piezoelectric force microscopy (PFM) images of the porous P(VDF-TrFE) film. For the PFM measurement, there is no conductive layer on top of the ferroelectric materials to clearly investigate the switching behavior [32,33]. Therefore, the porous P(VDF-TrFE) thin films were prepared on the n-Si / Ti / Au without the PEDOT:PSS layer unlike the solar cell structure. thin films of porous P(VDF-TrFE) were prepared on n-Si with Ti / Au back contacts. To investigate the ferroelectric properties of the film, such as the reversal capability or localized polarization, the samples for PFM measurements are fabricated without PEDOT: PSS layers. The film with 65% porosity was ~150 nm thick, being networked in such a way as to expose the Si surface inside the pores (Fig. 3**a and S4**). Fig. 3**b** shows the downward polarization PFM amplitude obtained by scanning a $3 \times 3\ \mu m^2$ porous film using a grounded tip, with a positive voltage applied to the bottom electrode. Line analysis of the PFM amplitude image (Fig. 3**c**) clearly shows that polarization is induced only in the networked P(VDF-TrFE) region (with the exception of pores). To confirm the polarization reversal capability of porous films (Fig. 3**d**), downward polarization was performed on a $3 \times 3\ \mu m^2$ area, with upward polarization performed on a smaller inner area of $1 \times 1\ \mu m^2$. As a result, the polarization reversal (Fig. 3**e and f**) was confirmed by the clear 180° phase shift relative to a clean P(VDF-TrFE) background with uniform downward polarization, indicating that the porous ferroelectric P(VDF-TrFE) film is suited for use as a solar cell interlayer.

Organic-inorganic hybrid solar cells based on *n*-type Si and PEDOT:PSS junctions have attracted increased attention due to their hole-selective transport at Schottky heterojunctions and the high transparency and hole conductivity of PEDOT:PSS [34–42]. The built-in electric field associated with Schottky junctions separates the photogenerated electrons and holes to create a photocurrent. Fig. 4**a** shows a schematic diagram of a PEDOT:PSS/P(VDF-TrFE)/Si organic-inorganic hybrid solar cell fabricated using a porous P(VDF-TrFE) film as an interlayer.

Although the ferroelectric layer strengthens the built-in electric field of the contacting Si, its insulating nature blocks the transport of charge carriers, implying that the porosity of this layer should be optimized. Therefore, we fabricated a series of hybrid solar cells with interlayers comprising P(VDF-TrFE) films of different porosity (from 0% in continuous thin films to 100% in non-ferroelectric ones), with the corresponding current density–voltage (*J–V*) curves and photovoltaic performances presented in Fig. S5 and Table S1, respectively, showing that both Photo conversion efficiency (PCE) and PCE enhancement (ΔPCE) before and after positive poling depend on the porosity of P(VDF-TrFE). Obviously, solar cells with continuous ferroelectric thin films as interlayers exhibit a negligible photovoltaic effect due to the insulating nature of P(VDF-TrFE) (Fig. S5**a**). As porosity increases, PCE and ΔPCE increase to their maximum values and then decrease. Specifically, the average PCE equals 11.4% at a porosity of 80%, whereas ΔPCE has a maximum value of 46.8% at a porosity of 40%. The maxima of PCE and ΔPCE are observed at different porosities, since the former parameter is approximately proportional to the area of the heterojunction between *n*-Si and PEDOT:PSS, thereby achieving its maximum at a relatively high porosity of ~ 80%. Conversely, ΔPCE is influenced by the additional electric field induced by the ferroelectric thin film in the peripheral region of the pores. As shown in Fig. S2, the above peripheral area is highest at a porosity of ~40%, since porosity is positively correlated with pore size. It is worth noting that solar cells with an interlayer porosity of 80% have a higher efficiency than ferroelectric interlayer–free ones with a layer porosity of 100%.

Fig. 4**b** shows the *J–V* curve of a hybrid solar cell with an interlayer of 80% porosity recorded at various poling voltages (Table 1). Poling of ferroelectric thin films was performed by applying an increasing voltage from 0 to 20 V in the positive direction at 5-V intervals and a voltage from –5 to −15 V in the negative direction (Table 1), with the negatively poled PEDOT:PSS/P(VDF-TrFE)/Si solar cell exhibiting J_{sc} = 28.7 mA cm^{-2}, V_{oc} = 532 mV, and FF = 53.2%, yielding a PCE of 8.40%. The lower V_{oc} and FF originate from the electron-hole recombination caused by negative ferroelectric layer poling. Upon positive poling at a voltage of +20 V, the PCE of the PEDOT:PSS/P(VDF-TrFE)/Si solar cell improved to 11.73%, with J_{sc} = 30.8 mA cm^{-2}, V_{oc} = 583 mV, and FF = 65.4%. This dramatic increase was attributed to the elevated amount of photogenerated charges due to reduced recombination, resulting in a performance enhancement of as much as 10% compared to the corresponding non-poled cell.

Fig. 4**c** shows the V_{oc} of the hybrid solar cell as a function of poling

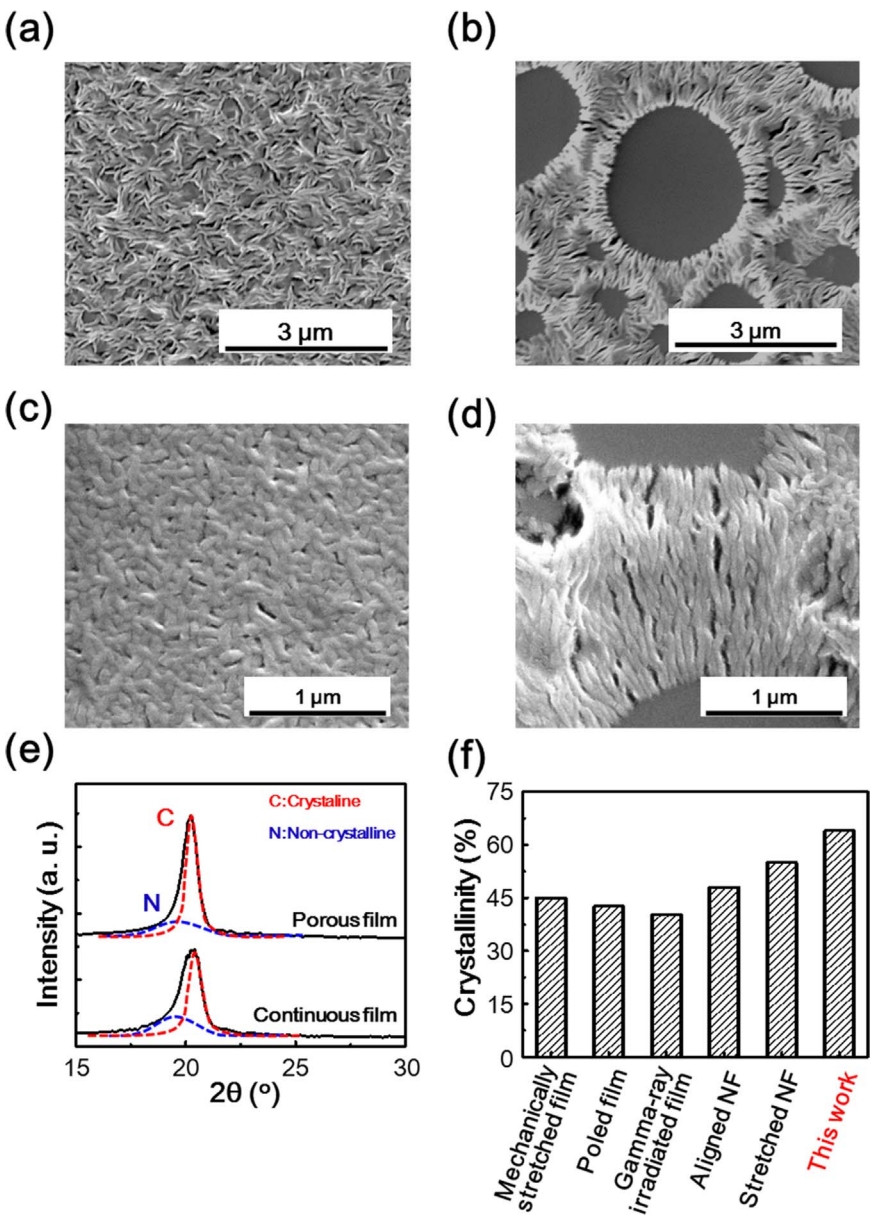

Fig. 2. High-magnification SEM images of (a,c) continuous and (b,d) porous P(VDF-TrFE) thin films. (e) XRD patterns of continuous and porous P(VDF-TrFE) thin films, (f) crystallinities of PVDF/P(VDF-TrFE) films prepared by methods reported elsewhere.

voltage. Regardless of the poling direction, V_{oc} rapidly changes in the region between –5 and 5 V and saturates at poling voltages above 5 V, suggesting that a 150-nm-thick P(VDF-TrFE) thin film can be sufficiently poled at a voltage of 5 V, i.e., at an electric field of ~33 MV/cm. Mai et al. [43]. measured the displacement–electric field (D–E) curves of P(VDF-TrFE) thin films prepared by spin coating and LB methods on Al bottom electrodes, showing that the coercive field of these films obtained from D–E hysteresis loops was inversely proportional to the film thickness, lying in the range of 43–127 MV/cm. These coercive fields were considerably larger than the poling voltage of the porous P(VDF-TrFE) thin film used in this study, which was ascribed to the different crystallinities of porous and continuous P(VDF-TrFE) thin films.

This poling effect is reversibly switchable from positive state and negative state, repeatedly. As shown in Fig. S6, the positively poled device exhibited 11.7% with J_{sc} = 29.7 mA cm^{-2}, V_{oc} = 580 mV, and FF = 68.0% at the first scan. Consecutively, the device is negatively poled as −15 V, and then showed 8.67% with J_{sc} = 28.2 mA cm^{-2}, V_{oc} = 550 mV, and FF = 55.9% at the second scan. When the devices are switched from positive poling state to negative poling state repeatedly, the efficiency is maintained around 11% after positive poling while efficiency is around 8.5% after negative poling. After each cycle, all the output parameter are reversible to similar levels.

Fig. S7 shows the V_{oc} changes of the devices with and without ferroelectric layers as a function of the time. Three photovoltaic devices (positively poled, non-poled, and without ferroelectric layer) were prepared and the poling was performed only once immediately after the fabrication of the device. The fabricated non poled device exhibited the V_{oc} of 563 mV (black line) while the device without ferroelectric interlayer showed V_{oc} of 570 mV (green line). On the other hands, positively poled devices show the V_{oc} of 587 mV (blue line). The PEDOT:PSS/n-Si based solar cells are known to be degraded rapidly due to the penetration of humidity into the junctions, resulting in the deterioration of V_{oc} [44]. Likewise, the V_{oc} of the all devices are decreased as the time passed (Fig. S7**a**). However, the degradation of the devices as time passed should be distinguished from poling duration. Specifically, the ΔV_{oc} (V_{oc} differences between non-poled and poled devices) corresponding to magnitude of the poling effect, is maintained until 12 h later while the V_{oc} is deteriorated as time passed. After 12 h, the ΔV_{oc} also start to be decreased (Fig. S7**b**). Consequently, the effect of poling is maintained until 12 h, and then slightly weakened. Additionally, because P(VDF-TrFE) layers can prevent the humidity

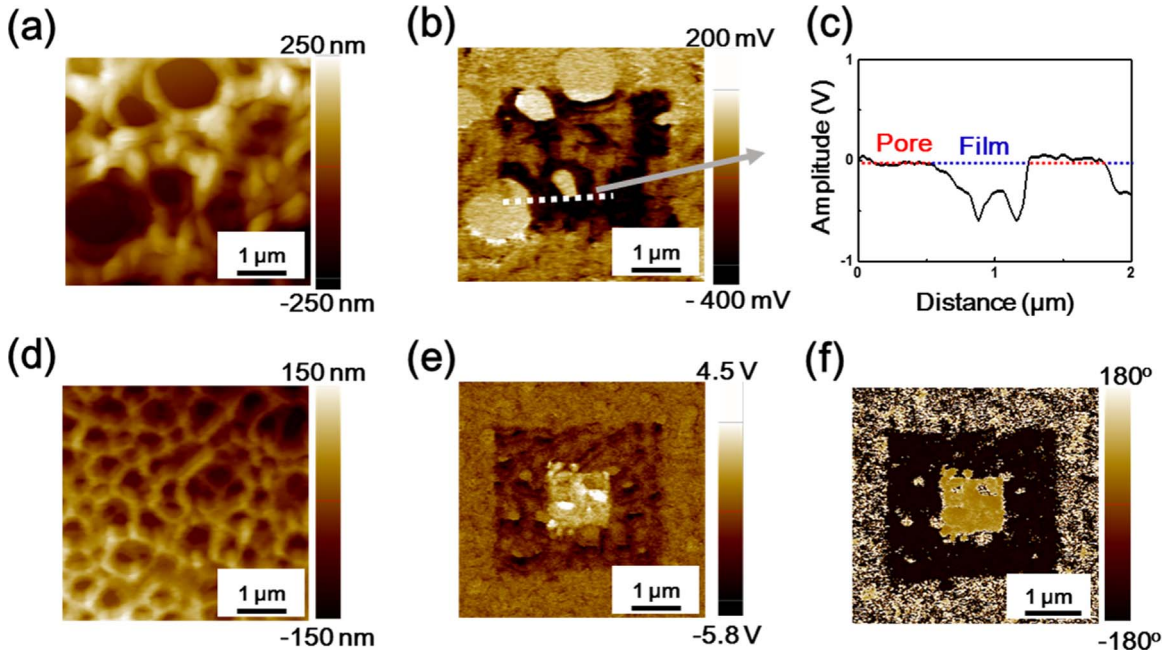

Fig. 3. AFM and piezoresponse images of a P(VDF-TrFE) porous film. (a) AFM topography, (b) PFM amplitude for a film with 65% porosity poled at +10 V over the central 3 × 3 μm^2 area. (c) Line scanning of PFM amplitude. (d) AFM topography, (e,f) PFM amplitude, and PFM phase for a film with 40% porosity poled at +10 and −10 V over 3 × 3 and 1 × 1 μm^2 areas, respectively.

penetration in to the junctions, the stability of the hybrid solar cell is also improved. The PEDOT:PSS/n-Si degrades from initially 565–503 mV while the V_{oc} of PEDOT:PSS/n-Si with ferroelectric layers is decreased from 587 mV to 536 mV.

The dark *J–V* curve is a good indicator of photovoltaic performance, with curves recorded for PEDOT:PSS/P(VDF-TrFE)/Si solar cells before

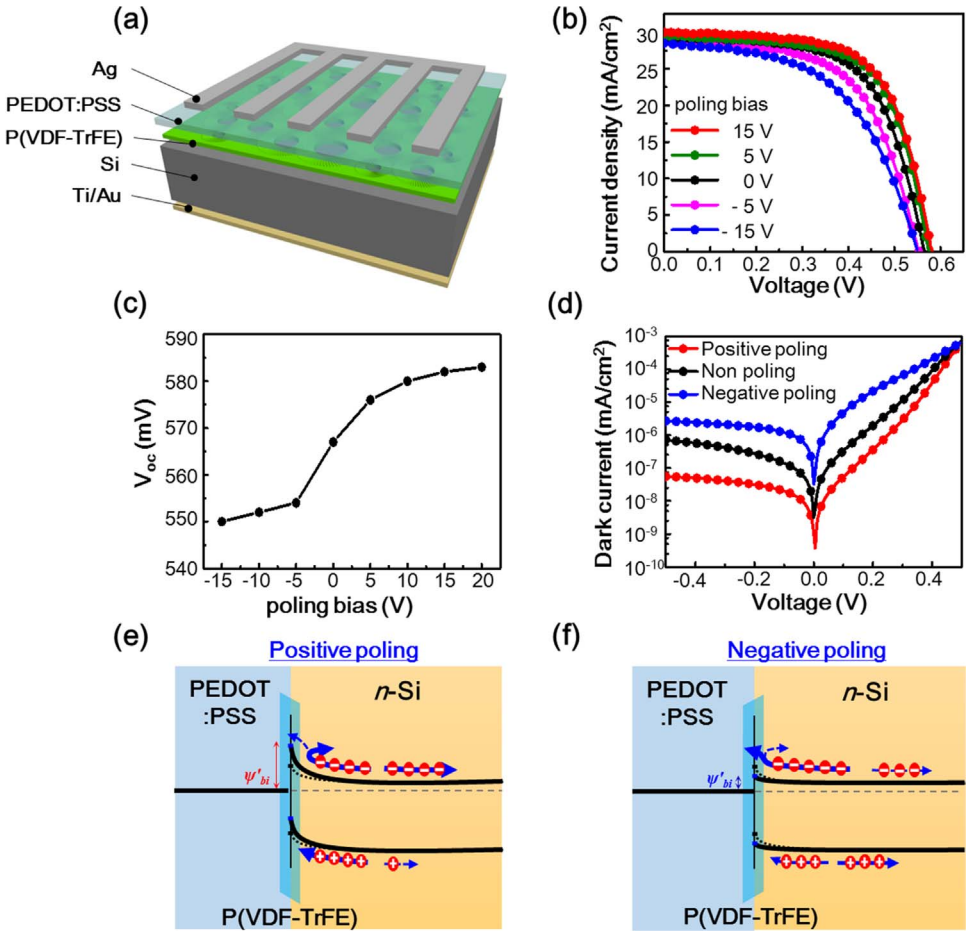

Fig. 4. (a) Schematic illustration of a PEDOT:PSS/P(VDF-TrFE)/Si solar cell and photovoltaic performance variation upon insertion of a porous P(VDF-TrFE) thin film between PEDOT:PSS and Si. (b) *J–V* curves for 1-sun-illuminated devices poled under different conditions. (c) Open circuit voltage as a function of poling voltage. (d) Dark *J–V* curves of devices subjected to positive poling (red line), no poling (black line), and negative poling (blue line). Band diagram and working principles of the porous ferroelectric P(VDF-TrFE) interlayer for hybrid solar cells under positive (e) and (f) negative poling conditions. (For interpretation of the references to color in this figure legend, the reader is referred to the web version of this article.)

Table 1
J-V characteristics of PEDOT:PSS / P(VDF-TrFE) / n-Si solar cells with poling voltage.

Poling voltage [V]	−15	−10	−5	0	5	10	15	20
V_{oc} [V]	0.55	0.552	0.554	0.567	0.576	0.58	0.582	0.583
J_{sc} [mA/cm^2]	28.7	29.2	29.5	29.9	30.2	30.3	30.6	30.8
FF [%]	53.2	57.5	59.2	62.5	65.0	65.0	65.1	65.4
Efficiency [%]	8.40	9.25	9.67	10.58	11.30	11.44	11.59	11.73

Table 2
Reverse saturation current density (Js) and ideality factor (n) of PEDOT:PSS/P(VDF-TrFE)/Si solar cell before and after poling.

	Js (A)	n (average)
Negative poling	3.22E-8	2.87
Non poling	3.17E-9	2.03
Positive poling	1.05E-9	1.67

and after poling shown in Fig. 4**d**. After positive poling, the dark saturation current decreased by more than one order of magnitude, increasing upon negative poling (Table 2), which can be explained using the energy band diagram for the heterojunction of *n*-Si and PEDOT:PSS with a poled P(VDF-TrFE) interlayer. The above junction was assumed to be of the Schottky type due to being similar to metal-semiconductor junctions, with PEDOT:PSS acting as a metal due to its high work function. In this junction, the built-in potential ψ_{bi} at the metal-semiconductor junction is ideally defined as the difference between the PEDOT:PSS work function $q\phi_P$ and the electron affinity of Si with a band energy of $q\chi_S + (E_C - E_F)$. During thermal equilibrium establishment, electrons move from the *n*-type semiconductor to the metal, causing upward band bending in *n*-type Si. The presence of porous P(VDF-TrFE) at the *n*-Si/PEDOT:PSS interface affects the above band bending depending on the direction of its ferroelectric polarization. For positive poling (Fig. 4**e**), the upward band bending of *n*-Si is increased, resulting in a decreased reverse saturation current flowing from PEDOT:PSS to Si. Conversely, for negative poling, the band bending of *n*-Si is reduced, resulting in a nearly flat band state and increasing the reverse saturation current (Fig. 4**f**).

The open circuit voltage depends on the saturation current J_0 and the light-generated current J_L of the solar cell (Eq. (1)) [45]. Since J_L does not typically exhibit large variations, the key influence is exerted by J_0, since this quantity can be varied by several orders of magnitude, as demonstrated herein.

$$V_{OC} = \frac{nkT}{q} \ln\left(\frac{J_L}{J_0}+1\right), \quad (1)$$

where n is the diode ideality factor, k is the Boltzmann constant, T is the absolute temperature, and q is a charge of an electron. According to Eq. (1), the saturation current decrease is responsible for the increase of V_{oc} after positive poling. Ideality factors obtained by linear fitting of *J–V* curves in the forward bias region are summarized in Table 2, decreasing in the order of negative poling > no poling > positive poling. After positive poling, the above parameter equaled 1.67, being close to unity and thus implying that the recombination of electrons and holes at the *n*-Si/PEDOT:PSS interface is retarded. This observation can be explained by the fact that photogenerated electrons and holes are efficiently collected rather than being trapped by interfacial states between *n*-Si and PEDOT:PSS, reducing the ideality factor to 1.0 and increasing the fill factor of the positively poled solar cell.

FDTD simulation was performed to more clearly understand the effect of porous ferroelectric thin films on the photovoltaic performance of hybrid solar cells (Fig. 5). The geometry of the PEDOT:PSS/P(VDF-TrFE)/Si hybrid solar cell considered in this simulation is shown in Fig. 5b, featuring island-shaped ferroelectric interlayers inserted at the interface between n-Si and PEDOT:PSS. Moreover, the calculations were performed assuming a poled ferroelectric material which has the remnant polarization of 100 mCm^{-2} (detailed in derivation S1, Supporting information). The PEDOT:PSS/Si hybrid solar cell without a ferroelectric layer was calculated to exhibit a moderate built-in potential of ~0.7 V induced by electrostatic potential energy differences, in good agreement with experimental data (Figs. 5**a and** 5**c**) [46]. However, after the ferroelectric thin film was inserted between *n*-Si and PEDOT:PSS, the built-in potential increased (Fig. 5**b** and **c**). Specifically, the electric field strength increased not only directly beneath ferroelectric islands (path “C” in Fig. 5**c**) but also in the peripheral regions of these islands not covered by the ferroelectric layer (path “B” in Fig. 5**c**), increasing the separation of photogenerated electron-hole pairs. Moreover, these photo generated carriers flatten the shape of the Schottky junction, the ferroelectric layers help to flow photo generated carriers and prevent recombinations. The efficient charge separation at the interface shortens the time required for the photogenerated carriers to stay at this interface, increasing their probability of being collected at the corresponding electrodes without recombining via interfacial states between *n*-Si and PEDOT:PSS.

6. Conclusion

We developed a *modified* BF technique to fabricate porous ferroelectric P(VDF-TrFE) thin films by spin coating a solution of P(VDF-TrFE) in acetone containing a small amount of deionized water. XRD, FT-IR and PFM measurements revealed that porous P(VDF-TrFE) thin films exhibit superior crystallinity and ferroelectric properties compared to those of continuous P(VDF-TrFE) thin films, which is ascribed to the reinforced crystallinity and ferroelectricity of the former due to the alignment and stacking of fibrous domains in the radial direction of the pores. The photovoltaic properties of a PEDOT:PSS/Si hybrid solar cell with a porous P(VDF-TrFE) interlayer were demonstrated to be

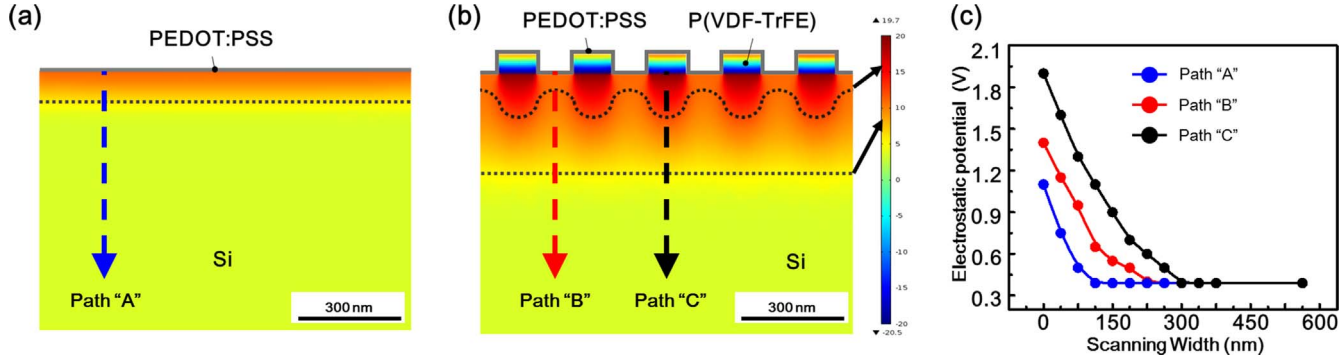

Fig. 5. FDTD electrostatic potential simulation for (a) PEDOT:PSS/*n*-type Si solar cell and (b) PEDOT:PSS/*n*-type Si solar cell with a ferroelectric layer; (c) line scans along paths A, B, and C.

reversibly switchable by repetitive positive and negative poling, and the optimized ferroelectric solar cell showed a PCE of 11.73%, which was more than 10% higher than that of a interlayer–free solar cell. FDTD simulation clearly indicated that the ferroelectric interlayer increases the strength of the built-in electric field between *n*-Si and PEDOT:PSS, promoting the separation of photogenerated electron-hole pairs and thereby suppressing their recombination. Compared to the conventional LB method, the modified BF technique is very useful for synthesizing substrate-supported porous polymeric thin films by spin coating, being widely applicable to various organic-inorganic hybrid devices.

Acknowledgements

This research was supported by Leading Foreign Research Institute Recruitment Program through the National Research Foundation of Korea (NRF) funded by the Ministry of Science and ICT (MSIP) (No. 2017K1A4A3015437), and this work was also supported by the Korea Institute of Energy Technology Evaluation and Planning (KETEP) and the Ministry of Trade, Industry & Energy of the Republic of Korea (No. 20163010012450).

Appendix A. Supporting materials

Supporting data associated with this article can be found in the online version at

Appendix B. Supporting information

Supplementary data associated with this article can be found in the online version at http://dx.doi.org/10.1016/j.nanoen.2017.09.033.

References

[1] S. Fujisaki, H. Ishiwara, Y. Fujisaki, Appl. Phys. Lett. 90 (2007) 185013.
[2] K.N.N. Unni, R. de Bettignies, S. Dabos-Seignon, J.M. Nunzi, Appl. Phys. Lett. 85 (2004) 1823–1825.
[3] M.Y. Li, H.J. Wondergem, M.J. Spijkman, K. Asadi, I. Katsouras, P.W.M. Blom, D.M. de Leeuw, Nat. Mater. 12 (2013) 433–438.
[4] L.H. Fan, J.L. Harris, F.A. Roddick, N.A. Booker, Water Res. 35 (2001), pp. 4455–4463.
[5] S. Srisurichan, R. Jiraratananon, A.G. Fane, J. Membr. Sci. 277 (2006) 186–194.
[6] J.F. Hester, P. Banerjee, A.M. Mayes, Macromolecules 32 (1999) 1643–1650.
[7] C.H. Lang, J. Fang, H. Shao, H.X. Wang, G.L. Yan, X. Ding, T. Lin, Nano Energy 35 (2017) 146–153.
[8] X.H. Ren, H.Q. Fan, C. Wang, J.W. Ma, S.H. Lei, Y.W. Zhao, H. Li, N.S. Zhao, Nano Energy 35 (2017) 233–241.
[9] M. Choi, G. Murillo, S. Hwang, J.W. Kim, J.H. Jung, C.Y. Chen, M. Lee, Nano Energy 33 (2017) 462–468.
[10] W.J. Song, S.H. Joo, D.H. Kim, C. Hwang, G.Y. Jung, S. Bae, Y. Son, J. Cho, H.K. Song, S.K. Kwak, S. Park, S.J. Kang, Nano Energy 32 (2017) 255–262.
[11] Z. Lou, S. Chen, L.L. Wang, K. Jiang, G.Z. Shen, Nano Energy 23 (2016) 7–14.
[12] F. Xia, H.S. Xu, B. Razavi, Q.M. Zhang, Mater. Res. Soc. Symp. P 665 (2002) 407–412.
[13] S.J. Kang, Y.J. Park, I. Bae, K.J. Kim, H.C. Kim, S. Bauer, E.L. Thomas, C. Park, Adv. Funct. Mater. 19 (2009) 2812–2818.
[14] W. Zeng, X.M. Tao, S. Chen, S.M. Shang, H.L.W. Chan, S.H. Choy, Energ. Environ. Sci. 6 (2013) 2631–2638.
[15] W.T. Liu, X.Y. Cheng, X. Fu, C. Stefanini, P. Dario, Microelectron. Eng. 88 (2011) 2251–2254.
[16] S.B. Kang, S.H. Won, M.J. Im, C.U. Kim, W.I. Park, J.M. Baik, K.J. Choi, Nanotechnology 28 (2017) 395402.
[17] Y.B. Yuan, T.J. Reece, P. Sharma, S. Poddar, S. Ducharme, A. Gruverman, Y. Yang, J.S. Huang, Nat. Mater. 10 (2011) 296–302.
[18] Y.B. Yuan, P. Sharma, Z.G. Xiao, S. Poddar, A. Gruverman, S. Ducharme, J.S. Huang, Energ. Environ. Sci. 5 (2012) 8558–8563.
[19] W. Regan, S. Byrnes, W. Gannett, O. Ergen, O. Vazquez-Mena, F. Wang, A. Zettl, Nano Lett. 12 (2012) 4300–4304.
[20] D. Sarazin, C. Picot, S. Patlazhan, Macromolecules 39 (2006) 1226–1233.
[21] J.Y. Ding, A.J. Zhang, H. Bai, L. Li, J. Li, Z. Ma, Soft Matter 9 (2013) 506–514.
[22] H. Bai, C. Du, A.J. Zhang, L. Li, Angew. Chem. Int. Ed. 52 (2013) 12240–12255.
[23] A. Munoz-Bonilla, E. Ibarboure, E. Papon, J. Rodriguez-Hernandez, Langmuir 25 (2009) 6493–6499.
[24] S.J. Kang, Y.J. Park, J. Hwang, H.J. Jeong, J.S. Lee, K.J. Kim, H.C. Kim, J. Huh, C. Park, Adv. Mater. 19 (2007) 581.
[25] C. Harnagea, M. Alexe, J. Schilling, J. Choi, R.B. Wehrspohn, D. Hesse, U. Gosele, Appl. Phys. Lett. 83 (2003) 1827.
[26] L. Zhang, S. Ducharme, J. Li, Appl. Phys. Lett. 91 (2007) 123974.
[27] A. Salimi, A.A. Yousefi, Polym. Test. 22 (2003) 699–704.
[28] V. Sencadas, S. Lanceros-Mendez, J.F. Mano, Thermochim. Acta 424 (2004) 201–207.
[29] M.H.A. Rahaman, M.U. Khandaker, Z.R. Khan, M.Z. Kufian, I.S.M. Noor, A.K. Arof, Phys Chem Chem Phys 16 (2014) 11527–11537.
[30] L. Persano, C. Dagdeviren, Y.W. Su, Y.H. Zhang, S. Girardo, D. Pisignano, Y.G. Huang, J.A. Rogers, Nat. Commun. 4 (2013) 1633.
[31] C.H. Du, B.K. Zhu, Y.Y. Xu, J. Appl. Polym. Sci. 104 (2007) 2254–2259.
[32] B.B. Tian, J.L. Wang, S. Fusil, Y. Liu, X.L. Zhao, S. Sun, H. Shen, T. Lin, J.L. Sun, C.G. Duan, M. Bibes, A. Barthe´le´my, B. Dkhil, V. Garcia, X.J. Meng, J.H. Chu, Nat. Comm. 7 (2016) 11502.
[33] Z. Wen, C. Li, D. Wu, A. Li, N. Ming, Nat. Mater. 12 (2013) 617–621.
[34] J. Zhang, T. Song, X.L. Shen, X.G. Yu, S.T. Lee, B.Q. Sun, ACS Nano 8 (2014) 11369–11376.
[35] J.Y. Chen, C. Con, M.H. Yu, B. Cui, K.W. Sun, ACS Appl. Mater. Interfaces 5 (2013) 7552–7558.
[36] H.M. Zhao, D. Xie, T.T. Feng, Y.F. Zhao, J.L. Xu, X.M. Li, H.W. Zhu, T.L. Ren, Appl. Phys. Express 7 (2014) 031603.
[37] L.N. He, C.Y. Jiang, H. Wang, D. Lai, Rusli, Appl. Phys. Lett. 100 (2012) 073503.
[38] N. Ikeda, T. Koganezawa, D. Kajiya, K. Saitow, J. Phys. Chem. C 120 (2016) 19043–19048.
[39] H.J. Syu, S.C. Shiu, C.F. Lin, Sol. Energy. Mater. Sol. Cells 98 (2012) 267–272.
[40] Q.M. Liu, T. Ohki, D.Q. Liu, H. Sugawara, R. Ishikawa, K. Ueno, H. Shirai, Nano Energy 11 (2015) 260–266.
[41] L. Mao, Q. Chen, Y.W. Li, Y. Li, J.H. Cai, W.M. Su, S. Bai, Y.Z. Jin, C.Q. Ma, Z. Cui, L.W. Chen, Nano Energy 10 (2014) 259–267.
[42] X.H. Mu, X.G. Yu, D.K. Xu, X.L. Shen, Z.H. Xia, H. He, H.Y. Zhu, J.S. Xie, B.Q. Sun, D.R. Yang, Nano Energy 16 (2015) 54–61.
[43] M.F. Mai, B. Martin, H. Kliem, J. Appl. Phys. 110 (2011) 064101.
[44] J. Schmidt, V. Titova, D. Zielke, Appl. Phys. Lett. 103 (2013) 183901.
[45] K. Bouzidi, M. Chegaar, A. Bouhemadou, Sol. Energy Mater. Sol. Cells 91 (2007) 1647–1651.
[46] S. Jackle, M. Mattiza, M. Liebhaber, G. Bronstrup, M. Rommel, K. Lips, S. Christiansen, Sci. Rep. 5 (2015) 13008.

Sung Bum Kang is a Ph.D course candidate under the supervision of Prof. Kyoung Jin Choi at School of Materials Science and Engineering, Ulsan National Institute of Science and Techonology (UNIST). His research focuses on development of polymeric ferroelectric nanostructures for piezoelectric energy harvesting, solar cell and fundamental study.

Myeong Hoon Jeong is a Ph.D course candidate under the supervision of Prof. Kyoung Jin Choi at School of Materials Science and Engineering, Ulsan National Institute of Science and Techonology (UNIST). His research interested is focused on LEDs, thermoelectric and solar cells

In young Choi is a master course student under the supervision of Prof. Kyoung Jin Choi at School of Materials Science and Engineering, Ulsan National Institute of Science and Techonology (UNIST). Her research interested is focused on high efficiency solar cells

So-Dam Sohn is a Ph.D course candidate under the supervision of Prof. Hyung-Joon Shin at School of Materials Science and Engineering, Ulsan National Institute of Science and Techonology (UNIST). Her research interested is focused on Atomic force microspcopy and its measurement.

Su Han Kim received his B.S. Degree in 2014 from Hanyang University, Seoul, Korea. He is studying for a doctor's degree under the supervision of Prof. W. I. Park in Hanyang University. His research mainly focuses on the synthesis of 2D materials and its applications in electronic and optoelectronic devices.

Dr. Hyung-Joon Shin is now associate Professor in School of Materials Science and Engineering, Ulsan National Institute of Science and Technology (UNIST). He received his Ph.D. from Materials Science and Engineering, Seoul National University in 2001. His recent research interest is focused on Electronic and geometric structure of nanomaterials. Scanning Tunneling Microscopy and Scanning Tunneling Spectroscopy, local modification of the electronic properties in nanoscale, and dynamics of single molecules on ultrathin insulating films.

Dr. Won Il Park is an associate professor in material science and engineering, Hanyang University. He received his Ph.D. degree in Material Sciences and Engineering from POSTECH in 2005, and joined Liber group of Harvard University as a postdoc fellow from 2005 to 2007. His present research interests are synthesis and characterization of semiconductor nanostructures such as nanowires, nanorods and 2D materials and development of nanoscale photonic and electronic devices.

Dr. Jae Cheol Shin is now assistant Professor in department of physics, Yeungnam university. He received his Ph.D. from University of Wisconsin-Madison in 2010. His recent research interest is focused on crystal growth of semiconductor structrues, lasers, photodetector, and optical and electrical deivces.

Dr. Myoung Hoon Song is now associate Professor in School of Materials Science and Engineering, Ulsan National Institute of Science and Technology (UNIST). He received his Ph.D. from Tokyo Institute of Technology (TIT) in 2005. His recent research interest is focused on organic and perovskite LED and solar cells.

Dr. Kyoung Jin Choi is now associate Professor in School of Materials Science and Engineering, Ulsan National Institute of Science and Technology (UNIST). He received his Ph.D. from Pohang University in Department of Materials Science and Engineering in 2001. His recent research interest is focused on nano-structures solar cell: semiconductor nanowires, quantum dots, Photoelectrochemical(PEC) water splitting based on visible-light photocatalysts and piezoelectric & thermoelectric energy harvester.